Kovove Mater. 51 2013 173–181
DOI: 10.4149/km_2013_3_173

Thermal, electrical, microstructure and microhardness properties of the eutectic Sn-3.5wt.%Ag alloy

F. Meydaneri[1]*, B. Saatçi[2], M. Özdemir[3]

[1]*Karabük University, Faculty of Engineering, Department of Metallurgy and Materials Engineering, 78050, Karabük, Turkey*
[2]*Erciyes University, Faculty of Sciences, Department of Physics, 38039, Kayseri, Turkey*
[3]*Erciyes University, Faculty of Sciences, Department of Chemistry, 38039, Kayseri, Turkey*

Received 31 January 2012, received in revised form 12 October 2012, accepted 17 October 2012

Abstract

The variation of thermal conductivity with temperature for Sn-3.5wt.%Ag eutectic alloy was measured with a radial heat flow apparatus. The thermal conductivity of the solid phase and temperature coefficient were also found to be 84.60 ± 0.09 W K^{-1} m^{-1} and 5.92×10^{-4} K^{-1}, respectively. The values of enthalpy of fusion (ΔH) and the specific heat (C_{P}) were also determined by differential scanning calorimeter (DSC) from heat flow curves during the transformation from eutectic solid to eutectic liquid. The variation of electrical conductivity with temperature for Sn-3.5wt.%Ag eutectic alloy was determined from the Wiedemann-Franz law by using the measured values of thermal conductivity. The microhardness of Sn-3.5wt.%Ag eutectic alloy was measured at approximately 5 different points with Vickers microhardness device. The microstructure of Sn-3.5wt.%Ag eutectic alloy was investigated by using scanning electron microscopy (SEM) and energy dispersive X-ray (EDX) analysis.

K e y w o r d s: metals & alloys, electrical resistivity/conductivity, microstructure, thermodynamics, hardness test

1. Introduction

Lead-tin alloys have been used as soldering materials for a long time. However, lead is a heavy poisonous metal and can be harmful to human health. The European Union (EU) has promulgated directives on July 1, 2006, to restrict the use of Pb in electronic products. Thus, there is an urgent demand for lead-free solders in the electronic industry. A low processing temperature is desirable for preventing heat damage to electronic devices during soldering, and this is the reason for the adoption of other low melting temperature alloys, i.e., Sn-Ag binary alloy and Ag-Sn based ternary alloys [1–14]. Information on interfacial reaction between solder and substrate is fundamentally important for the reliability evaluation of electronic joints. Among these Sn-based alloys, Sn-Ag alloy is one of the most promising candidates for Pb-free solder [15–18]. There are many studies dedicated to the study of mechanical properties of lead-free solder materials, including tensile properties, better ductility, higher strength superior resistance to creep and thermal fatigue, under different conditions [19–24]. One of its advantages is that they melt at temperatures near 221 ℃ instead of 183 ℃ like the eutectic Sn-37wt.%Pb alloy does. This property has led to higher service temperature applications. Other important properties are strength and ductility. The strength and ductility of a solder joint are very important for the service applications. Solder joints need to demonstrate a good balance between strength and ductility in order to withstand thermal, mechanical, and thermo-mechanical loading.

The knowledge of the thermodynamics of materials provides fundamental information about the stability of phases, the driving forces for chemical reactions and diffusion processes. Electrical conductivity data have great importance on the development of electronic

*Corresponding author: tel.: +90 370 433 20 21/1437; fax: +90 370 433 32 90; e-mail address: meydaneri@yahoo.com

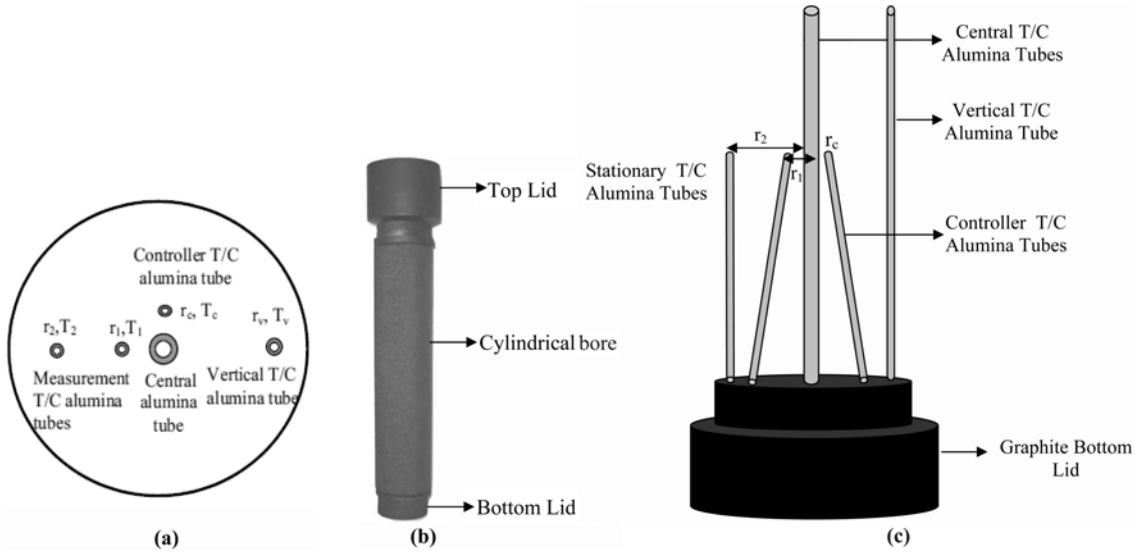

Fig. 1. (a) Transverse section of the sample. (b) Graphite crucible. (c) Longitudinal section of a part of the sample at the center of the specimen.

materials, interconnection technologies, especially in microelectronics and modern industry. In most cases, mechanical properties are needed for industrial applications, so the strength and hardness of alloys mainly depend on their microstructure. Thus, the purpose of present work is to determine the thermal and electrical conductivity, the enthalpy of fusion, the change of specific heat, microstructure, microhardness for Sn-3.5wt.%Ag eutectic alloy.

2. Materials and methods

2.1. Measurement of thermal conductivity of solid phases

The sample crucible is composed of three parts. A cylindrical bore, the top and bottom lids, which were tightly fitted to the cylindrical part, are shown in Fig. 1. There were four thermocouples placed on the bottom lid. The control (r_c) and the measurement thermocouple (r_1) holes were drilled at 86° angle to the ends of the cylinder tube. The measurement thermocouple (r_2) hole was placed to the back of the measurement thermocouple (r_1), namely ($r_2 > r_1$). A movable thermocouple was also placed 10 mm away from the center and used for measuring the vertical temperature variation. Also, a thin-walled central alumina tube was placed to isolate the central heating wire (Kanthal A1) on the bottom lid.

Then, the phase diagram of Sn-Ag system has been examined [25]. The Sn-3.5wt.%Ag eutectic alloy was molten within crucible made from graphite in a vacuum furnace by using 4N pure Sn, 4N pure Ag. After several stirring with a plunger, the molten material was poured into a graphite sample crucible held in a specially constructed casting furnace at approximately 50 K above the eutectic temperature, T_E, of the alloy (494 K). The molten metal was then directionally solidified from bottom to top to ensure that the sample crucible was completely full. The sample was prepared to be placed in the radial heat flow apparatus.

A radial heat flow apparatus was chosen to determine the thermal conductivity of solids because of its symmetrical properties. Originally, Gündüz and Hunt [26, 27] designed the radial heat flow apparatus, and Maraşlı and Hunt [28] improved the experimental apparatus for higher temperature, and the block diagram of the experimental system is shown in Fig. 2. The radial heat flow apparatus consists of a central heating element and a water cooling jacket. The central heating element was a 1.7 mm Kanthal A-1 wire inside a thin walled alumina tube and was used to heat specimen from the center. The water cooling jacket is made of stainless steel and was used to cool the outside of the specimen. To get radial heat flow, the specimen was heated from the center and the outside of the specimen was kept cool with the water cooling jacket. The temperature gradient on the specimen could be controlled by placing different materials into the gap between the specimen and the water cooling jacket.

The specimen was heated from the center using a single heating wire ($\sim$ 164 mm length and 1.7 mm in diameter, Kanthal A-1) in steps of 20 K up to 10 K below the melting temperature and the outside of the specimen was kept cool with the water cooling jacket to get a radial temperature gradient. The length of the central heating wire was chosen to be slightly longer than the length of the specimen to make the vertical isotherms parallel to the axis. The gap between the cooling jacket and the specimen was filled with free running sand to get a large radial temperature gradi-

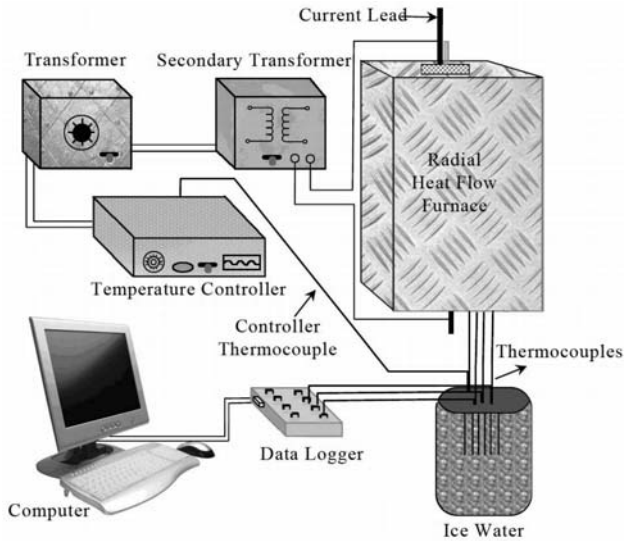

Fig. 2. Block diagram of radial heat flow system.

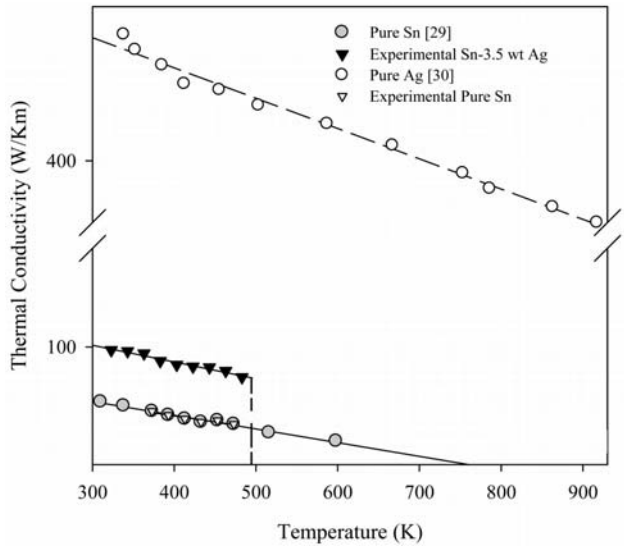

Fig. 3. Thermal conductivities of pure Sn [29], pure Ag [30] and eutectic Sn-3.5wt.%Ag alloy versus temperature.

ent on the specimen. The temperature of the specimen was controlled with Euroterm 9706 type controller and the temperature in the specimen was stable to ± 0.01–0.02 K for at least 2 h. At the steady state, the total input power and temperatures of the stationary thermocouples were recorded with Hewlett Packard 34401 type multimeter and Pico TC-08 model data logger. The vertical isotherm for each setting was made parallel to the axis at the measurement region by moving the central heater up and down. When the desired power setting and the temperature measurements had been completed during the heating process, the specimen was left to cool to the room temperature. Consider a cylindrical specimen heated by a heating element along the axis at the center of the specimen. At the steady-state conditions, the radial temperature gradient in the cylindrical specimen is given by Fourier's law

$$\left(\frac{\mathrm{d}T}{\mathrm{d}r}\right)_{\mathrm{S}} = -\frac{Q}{2\pi r \ell \kappa_{\mathrm{S}}}, \tag{1}$$

where Q is the total input power from the center of the specimen, and κ_{S} is the thermal conductivity of the solid phase. Integration of the Eq. (1) gives

$$\kappa_{\mathrm{S}} = \frac{1}{2\pi\ell} \ln\left(\frac{r_2}{r_1}\right) \frac{Q}{T_1 - T_2}, \tag{2}$$

where $a_0 = \dfrac{1}{2\pi\ell} \ln\left(\dfrac{r_2}{r_1}\right)$ is an experimental constant, ℓ is the length of the heating element, r_1 and r_2 are fixed distances from the center of the sample, and T_1 and T_2 are temperatures at the r_1 and r_2 fixed distances ($r_2 > r_1$), respectively:

$$\kappa_{\mathrm{S}} = a_0 \frac{Q}{T_1 - T_2}. \tag{3}$$

If the value of Q, r_1, r_2, ℓ, T_1 and T_2 can be accurately measured for the well-characterized sample crucible, then reliable κ_{S} values can be evaluated.

The sample was moved from the furnace. For the measurements of the r_1 and r_2, the specimen was cut transversely near the temperature measurement point. After that, the specimen was grounded and polished. The distances of the thermocouples from the center were then photographed with digital camera placed in conjunction with an Olympus BH2 optical microscope and a graticule ($100 \times 0.01 = 1$ mm) was also photographed using the same objective. The photographs of the distances of the thermocouples were superimposed on one another using Adobe PhotoShop CS2 version software, so that the distances of fixed thermocouples could be measured to an accuracy of $\pm$ 10 μm.

Experimental results for the thermal conductivity determination of solid phases for the Sn-3.5wt.%Ag eutectic alloy are given in Table 1. The variation of solid phase thermal conductivity is also shown in Fig. 3.

2.2. Determination of the temperature coefficient

The thermal temperature coefficient, α_{TTC}, can be obtained from the graph of thermal conductivity variations with the temperature, given in Table 2. κ_{S} is the

Table 1. Experimental data of the solid phase thermal conductivity for eutectic Sn-3.5wt.%Ag alloy

T (K)	Q (W)	T_1 (K)	T_2 (K)	ΔT (K)	κ_S (W K^{-1} m^{-1})
323	42.95	323.80	323.32	0.48	98.40
343	47.17	343.59	343.06	0.53	97.90
363	48.37	363.63	363.08	0.55	96.70
383	51.50	383.90	383.29	0.61	92.80
403	57.85	404.04	403.34	0.70	90.90
423	78.59	424.10	423.14	0.96	90.00
443	107.62	444.15	442.83	1.32	89.60
463	132.61	464.86	463.20	1.66	87.80
483	149.97	485.49	483.54	1.95	84.60

$r_1 = 0.462 \times 10^{-2}$ m, $r_2 = 1.524 \times 10^{-2}$ m, $\ell = 0.164$ m, $a_0 = 0.011 \times 10^{-2}$ m^{-1}

thermal conductivity of the solid phase at the temperature T, κ_{S0} is the thermal conductivity at the initial temperature T_0, and the thermal temperature coefficient α_{TTC} is written as [31]:

$$\alpha_{TTC} = \frac{\kappa_S - \kappa_{S0}}{\kappa_{S0}(T - T_0)} = \frac{1}{\kappa_{S0}} \frac{\Delta\kappa}{\Delta T}. \quad (4)$$

2.3. Measurement of electrical conductivity and electrical resistivity

For metallic conductors, current is carried by electrons. In this process, chemical properties of metal are not changed. The electrical conductivity (EC) is a measure of the ability to conduct an electric current, which is one of the physical properties of materials [32]. In other words, electrical conductivity is a measure of how well a material accommodates the movement of an electric charge. Electrical conductivity is a very useful property since values are affected by some properties such as the substances, chemical composition and the stress state of crystalline structures. Therefore, electrical conductivity information can be used for measuring purity of water, sorting materials, checking for proper heat treatment of metals, and inspecting for heat damage in some materials.

The connection between the thermal conductivity and the electrical conductivity is established by the Wiedemann-Franz law, given as

$$\sigma = \frac{\kappa_S}{LT}, \quad (5)$$

where σ is electrical conductivity, κ_S is the thermal conductivity of the solid phase at the temperature T, and L is the Lorenz number. This relationship is based upon the fact that both the heat and electrical transport involve free electrons in the metal. The value of L is 2.45×10^{-8} W Ω K^{-2}.

In present work, the variations of electrical conductivity versus temperature were determined from the Wiedemann-Franz law by using the values of κ_S and $L_{average}$. The values of L for pure materials are well-known, whereas it is unknown for alloys. To determine the variation of electrical conductivity with temperature from the Wiedemann-Franz law, the value of $L_{average}$ is also required as well as the values of κ_S. The Lorenz numbers for pure Ag and pure Sn are 2.37×10^{-8} and 2.49×10^{-8} W Ω K^{-2} [33], respectively. The average Lorenz value was used in the determination of electrical conductivity for Sn-Ag eutectic alloy since the values of Lorenz numbers for pure Ag and pure Sn are very close to each other. Electrical resistivity (also known as specific electrical resistance) is a measure of how strongly the material opposes the flow of electric current, and it is an intrinsic, bulk (not thin-film) property of a material. Electrical resistivity is inversely proportional to the electrical conductivity, and is given as

$$\rho = 1/\sigma. \quad (6)$$

The variations of electrical conductivity and resistivity versus temperature for Sn-3.5wt.%Ag eutectic alloy are shown in Figs. 4 and 5, respectively.

2.4. Determination of the electrical temperature coefficient

Electrical resistivity of metals increases with temperature, and electron-phonon interactions can play a key role. The conductivity and resistivity of material is temperature dependent. The conductivity of most materials decreases as temperature increases. Alternately, the resistivity of most materials increases with increasing temperature. The amount of change is material dependent but has been established for many elements and engineering materials. The reason that resistivity increases with increasing temperature is that the number of imperfection in the atomic lattice structure increases with temperature and this hampers electron movement. These imperfections include dislocations, vacancies, interstitial defects and impurity atoms [34].

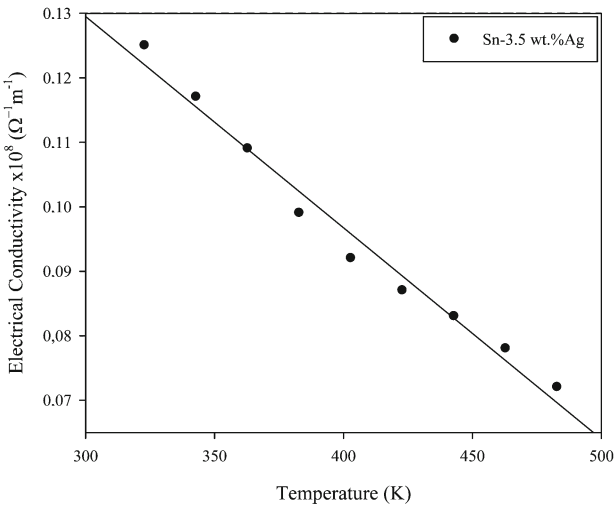

Fig. 4. The variation of electrical conductivity of the eutectic Sn-3.5wt.%Ag alloy versus temperature.

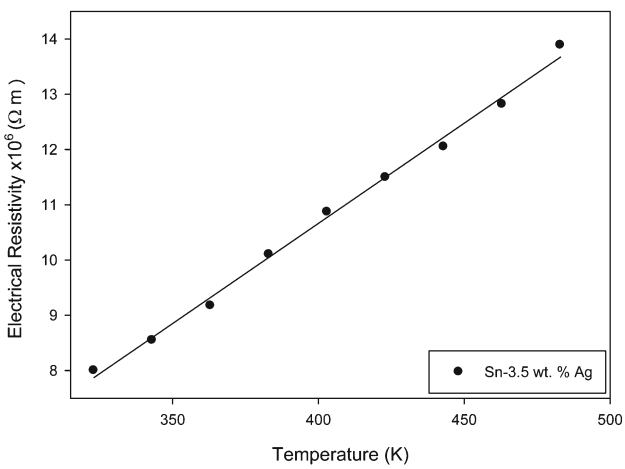

Fig. 5. The variation of electrical resistivity of the eutectic Sn-3.5wt.%Ag alloy versus temperature.

The dependence of electrical conductivity on temperature is often expressed as a slope in the electrical conductivity versus temperature graph and can be given as

$$\alpha_{\mathrm{ETC}} = \frac{1}{\sigma_0}\frac{\Delta\sigma}{\Delta T} = \frac{\sigma - \sigma_0}{\sigma_0(T - T_0)}, \tag{7}$$

where σ is the electrical conductivity of the solid phase at the temperature T, σ_0 is the electrical conductivity at the initial temperature T_0, and α_{ETC} is the electrical temperature coefficient. The electrical temperature coefficients for pure Sn, pure Ag and Sn-3.5wt.%Ag eutectic alloy were obtained from the graph of electrical conductivity variations with temperature and are also given in Table 2.

2.5. Determination of enthalpy and specific heat of fusion

Specific heat capacity is the quantity of heat required to raise a unit of substances masses temperature one degree Celsius. The specific heat capacity of a substance depends on its molecular structure and phase. Knowledge of the heat capacity of materials and the latent heat of phase transitions is needed to understand the thermodynamics of materials, their phase transitions, and they are very important parameters for industrial applications. For example, for measurements at constant pressure, the change in enthalpy is given by the temperature integral of the heat capacity. For most solids, at temperatures away from any phase transitions, the heat capacity is controlled by the vibrations of the atoms.

C_{p} = specific heat capacity at constant pressure,

$$C_{\mathrm{p}} = \left(\frac{\partial H}{\partial T}\right)_{\mathrm{p}}. \tag{8}$$

These data can be obtained by fitting the theoretical formula to the available experimental results and then using them for estimation of the considered properties in the whole temperature range (from 298.15 K to T_{melt}). Integration of Eq. (8) gives

$$H = \int_{298.15}^{T_{\mathrm{m}}} C_{\mathrm{p}}\mathrm{d}T. \tag{9}$$

At the melting temperature, the heat supplied to system will not rise its temperature but will be used in supplying the enthalpy of fusion (latent heat of melting) that is required to convert solid to liquid. For a transformation from solid state to liquid state, enthalpy of fusion can be expressed as

$$\Delta H \approx \Delta C_{\mathrm{p}} T_{\mathrm{M}}, \tag{10}$$

where T_{M} is the melting temperature, and ΔC_{p} is the change of specific heat. The DSC (Perkin Elmer Diamond model) thermal analysis was performed in the temperature range of 300–970 K with a heating rate of 10 K min^{-1} and under a constant stream of nitrogen at atmospheric pressure. The DSC curve obtained for Sn-3.5wt.%Ag eutectic alloy was shown in Fig. 6. The enthalpy of fusion (ΔH) was calculated as the area under the peak by numerical integration, and then the change of specific heat (ΔC_{p}) was determined by dividing the enthalpy of fusion to the melting temperature.

Table 2. Some thermal and electrical properties of the eutectic Sn-3.5wt.%Ag alloy

Sample (wt.%)	T (K)	κ ($\mathrm{W\,K^{-1}\,m^{-1}}$)	α_{TTC} ($\mathrm{K^{-1}}$)	$\sigma_0 \times 10^6$ ($\Omega^{-1}\,\mathrm{m^{-1}}$)	$\sigma \times 10^6$ ($\Omega^{-1}\,\mathrm{m^{-1}}$)	α_{ETC} ($\mathrm{K^{-1}}$)	$\rho_0 \times 10^{-8}$ (Ω m)	$\rho \times 10^{-8}$ (Ω m)	ΔH ($\mathrm{J\,g^{-1}}$)	ΔC_{p} ($\mathrm{J\,g^{-1}\,K^{-1}}$)
Sn-3.5Ag [36]	293	60.00–55.00	–	–	–	–	15.30	20.00	–	–
Sn-3.5Ag [37]	293–476	–	5.76×10^{-4}–6.80×10^{-4}	8.90	4.80	4.66×10^{-3}	11.20	20.70	59.10	0.260
Sn-3.5Ag [41]	493.4	–	–	–	–	–	12.30	–	60.20	–
Sn-3.5Ag [42]	300	–	–	–	–	–	7.70	–	–	–
Pure Sn [43]	300	–	–	–	–	–	12.00	–	–	–
Sn-3.5Ag [44]	293	–	–	–	–	–	12.30	–	–	–
Sn-3.5Ag [45]	–	–	–	–	–	–	–	15.40	–	–
Sn-3.5Ag [46]	–	–	–	–	–	–	–	16.80	–	–
Sn-3.5Ag [47]	494.3	–	–	–	–	–	–	–	–	0.220
Sn-3.5Ag [48]	498	–	–	–	–	–	–	–	67.00	–
Sn-3.5Ag [PW]	323–483	98.40–84.60	5.92×10^{-4}	12.50	7.20	3.32×10^{-3}	8.00	13.88	64.85	0.132

[PW]: Present Work

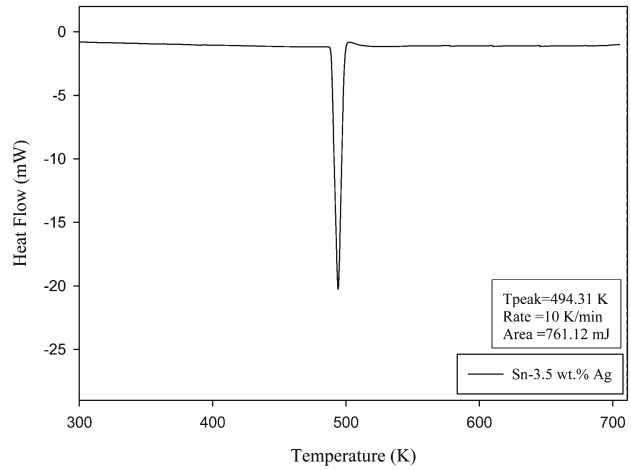

Fig. 6. Heat flow curve versus temperature for the eutectic Sn-3.5wt.%Ag alloy.

2.6. Microstructure, measurement of microhardness

Scanning electron microscope equipped with an energy dispersive X-ray (EDX) analysis system was used to inspect and analyze the microstructure of the sample and to perform the semi quantitative analysis on those structures in order to determine the phases. The microstructure of Sn-3.5wt.%Ag eutectic alloy was characterized by LEO 440 scanning electron microscope (SEM) equipped with an energy dispersive X-ray (EDX), and is also shown in Fig. 7.

The mechanical property such as the microhardness depends especially on the microstructure, processing temperature, the composition, etc. [35]. The mechanical properties of any solidified material are usually determined with hardness test, tensile strength test, ductility test, etc. Since true tensile strength testing of solidified alloys gave inconsistent results with a wide scatter due to the strong dependence on solidified sample surface quality, the mechanical properties were monitored by hardness testing, which is one of the easiest ways to determine the mechanical properties of the different phases of the structure. The microhardness measurement was done at room temperature by using hardness tester device (HMV-2 Micro Hardness Tester Shimadzu). The microhardness measured by Vickers method is defined as the ratio of the load applied (in kg) to the projected area of the indentation (in $\mathrm{mm^2}$). Vickers hardness measurement was performed to clarify the relationship between microstructure and microhardness. Vickers hardness value was obtained as

$$H_v = \frac{2F \sin \phi/2}{d^2}, \tag{11}$$

where ϕ is the indenter apex angle, F is the applied

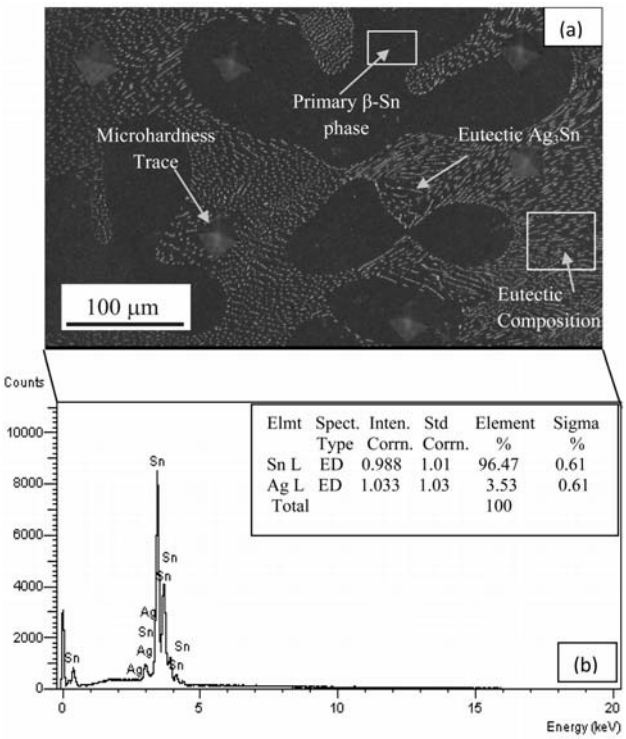

Fig. 7. (a) SEM micrograph and (b) EDX analysis of the eutectic Sn-3.5wt.%Ag alloy.

load, and d is the average length of diagonals. They were contacted by a square based pyramid diamond indenter, which is attached to a metallurgical microscope. Special attention was given to proper setting of the indenter on defined specimen surface. An optimum load value of 100 g was chosen and it was applied for 10 s to the sample. Indentations were made at five different places on sample to consider hardness variation. The accuracy of the microhardness measurement was about ± 5 %. Due to variation in crystallographic orientations of the specimen, the average value of microhardness was taken into account.

3. Results and discussion

3.1. The thermal conductivity and temperature coefficient

The eutectic melting temperature of Sn-3.5wt.%Ag eutectic alloy is about 494 K. The thermal conductivities of the solid phases, κ_S, versus temperature for pure Sn, pure Ag and Sn-3.5wt.%Ag eutectic alloy are shown in Fig. 3. The thermal conductivity of solid phases for the same material decreases with increasing temperature and the values of κ_S for Sn-3.5wt.%Ag eutectic alloy lie between the values of κ_S for pure Ag and pure Sn. The thermal conductivity of the solid phase and temperature coefficient for Sn-3.5wt.%Ag eutectic alloy at approximately its melting temperature were also found to be 84.60 ± 0.09 $\mathrm{W\,K^{-1}\,m^{-1}}$ and $5.92 \times 10^{-4}\,\mathrm{K^{-1}}$, respectively. κ_S values obtained with radial heat flow method in the present work are higher than κ_S values obtained with an automated device which measured jointly the electrical resistivity and the absolute thermoelectric power by Mhiaoui et al. [36]. The temperature coefficient ($5.92 \times 10^{-4}\,\mathrm{K^{-1}}$), calculated in the present work, agrees with the temperature coefficient (5.76×10^{-4}–6.80×10^{-4}) obtained at 293–476 K by Çadırlı et al. [37]. The temperature coefficient and thermal conductivity values obtained in literature and in the present work are given in Table 2.

3.2. The electrical conductivity, electrical resistivity and electrical temperature coefficient

The Lorenz numbers for pure Ag and pure Sn are 2.37×10^{-8} and 2.49×10^{-8} $\mathrm{W\,\Omega\,K^{-2}}$ [33], respectively. To determine the variation of electrical conductivity with temperature from the Wiedemann-Franz law for Sn-3.5wt.%Ag eutectic alloy, the average Lorenz value was used since the values of Lorenz numbers for pure Ag and pure Sn are very close to each other. The variations of electrical conductivity versus temperature for Sn-3.5.wt.%Ag eutectic alloy are shown in Fig. 4. The values of σ for Sn-3.5wt.%Ag eutectic alloy were obtained to be 12.50×10^6–7.20×10^6 $\mathrm{\Omega^{-1}\,m^{-1}}$ at the temperature range of 323–483 K. The electrical temperature coefficient for the same alloy was found to be $3.32 \times 10^{-3}\,\mathrm{K^{-1}}$ at the temperature range of 323–483 K. The electrical resistivity values (ρ) for the same alloy were found to be 8×10^{-8}–13.88×10^{-8} Ω m at the temperature range of 323–483 K. The electrical conductivity values (12.50×10^6–7.20×10^6 $\mathrm{\Omega^{-1}\,m^{-1}}$) determined from the Wiedemann-Franz law at 323–483 K in the present work are higher than the electrical conductivity values (8.90×10^6–4.80×10^6 $\mathrm{\Omega^{-1}\,m^{-1}}$) measured with the d.c. four-point probe method at 293–476 K by Çadırlı et al. [37], but the electrical temperature coefficient and the electrical resistivity values are close to our results. The electrical resistivity, electrical conductivity and electrical temperature coefficient values obtained in literature and in present work are given in Table 2.

3.3. Determination of enthalpy of fusion and the change of specific heat

Sn-3.5wt.%Ag eutectic alloy was heated with a heating rate of 10 K $\mathrm{min^{-1}}$ at the temperature range of 300–970 K by using a Perkin Elmer Diamond model DSC, and the heat flow versus temperature

for Sn-3.5wt.%Ag eutectic alloy is given in Fig. 6. As can be seen from Fig. 6, the melting temperature of Sn-3.5wt.%Ag eutectic alloy was detected to be 494.31 K. The value of the enthalpy of fusion (ΔH) and the change of specific heat (ΔC_p) for Sn-3.5wt.%Ag eutectic alloy were also calculated to be 64.85 J g^{-1} and 0.132 J g^{-1} K^{-1}, respectively, from the graph of the heat flow versus temperature. In literature, values of enthalpy of fusion for Ag and Sn are 104.76 and 58.90 J g^{-1} [38, 39], respectively, and the values of specific heat change for pure Ag and Sn are 0.235 and 0.117 J g^{-1} K^{-1}, respectively. The values of enthalpy of fusion (ΔH) found in the present work are very close to the values (ΔH) obtained in literature, but the change of specific heat (ΔC_p) is lower than the others. The enthalpy of fusion (ΔH) and the change of specific heat (ΔC_p) obtained in literature and in the present work are given in Table 2.

3.4. Microstructure and microhardness of the composition

The results showed that the addition of silver to pure tin caused more precipitations of the intermetallic compound Ag_3Sn. According to the corresponding sample, it can be seen that the eutectic structure consists of a mixture of intermetallic compounds Ag_3Sn and β-Sn phase and the eutectic reaction is $L \rightarrow Ag_3Sn + \beta$-Sn. The samples show clear dendritic structures. In Fig. 7, it is shown that large dark gray dendrites are primary β-Sn phase surrounded by a net-like eutectic mixture of β-Sn phase and Ag_3Sn.

The microhardness (Hv0.1) for eutectic Ag_3Sn and primary β-Sn phases in Sn-3.5wt.%Ag alloy was measured from approximately 5 different points with Vickers microhardness device. The microhardness values for eutectic Ag_3Sn phase were obtained to be 11.6, 12.4, 14.5, 12.8, 14.7, and the average microhardness value (Hv0.1) of eutectic Ag_3Sn phase was calculated to be 13.20 ± 0.6 kg mm^{-2}. The microhardness values for primary β-Sn phase were obtained to be 8.8, 9.7, 9.1, 7.4, 7.7, and the average microhardness value (Hv0.1) of primary β-Sn phase was calculated to be 8.54 ± 0.4 kg mm^{-2}. In general, the hardness of Sn-based alloys strongly depends on the alloying element; the higher the alloying element is, the higher the hardness is. In literature, the value of Vickers microhardness of pure Sn was given to be 5 kg mm^{-2} [40]. As can be seen from Fig. 7, eutectic mixture of β-Sn phase and intermetallic Ag_3Sn phase surrounded dendritic primary β-Sn phase, and strength of sample was increased. As a result, the Vickers hardness test shows that fine β-Sn and spherical Ag_3Sn phases strongly improve the microhardness of the Sn-3.5wt.%Ag solder.

4. Conclusions

The main conclusions of this investigation may be summarized as follows:

In previous studies, thermal conductivity values of Sn-Ag eutectic alloy were estimated from measuring the electrical conductivities and using the Wiedemann-Franz law. In the present study, on the contrary, electrical conductivities of eutectic Sn-Ag alloy were estimated from measuring the thermal conductivity values and using the Wiedemann-Franz law. The thermal conductivity variation for eutectic Sn-3.5wt.%Ag alloy was investigated by using a radial heat flow apparatus. The thermal temperature coefficient for the eutectic Sn-3.5wt.%Ag alloy was determined from the graph of the thermal conductivity variations with temperature. The temperature coefficient of electrical conductivity for the sample was determined from the graph of electrical conductivity variation with temperature. The enthalpy of fusion (ΔH) and the change of specific heat (ΔC_p) for eutectic Sn-3.5wt.%Ag lead-free solder alloy were also found from the graph of the heat flow versus temperature. Microstructure of eutectic Sn-3.5wt.%Ag alloy was investigated by SEM. Composition analysis of the same sample was determined with EDX. Microhardness measurement on composition was made with Vickers microhardness tester device and average values were calculated.

Acknowledgements

This project was supported by the Erciyes University Scientific Research Project Unit under Contract No: FBD-09-846. Authors would like to thank the Erciyes University Scientific Research Project Unit for its financial support. The authors also thank Assoc. Prof. Dr. Dursun Özyürek for his valuable discussions and his help.

References

[1] Lee, C., Lin, C., Y., Yen, Y. W.: J. Alloy Compd., *458*, 2008, p. 436. doi:10.1016/j.jallcom.2007.04.002
[2] Rae, A., Handwerker, A.: Circuits Assembly, 2004, p. 20.
[3] Puttlitz, K. J., Stalter, K. A.: Handbook of Lead-Free Solder Technology for Microelectronic Assemblies. New York, Marcel Dekker 2004, p. 239. doi:10.1201/9780203021484
[4] Wang, C. H., Chen, S.-W.: Acta Mater., *54*, 2006, p. 247. doi:10.1016/j.actamat.2005.09.006
[5] Hassama, S., Baharib, Z., Legendre, B.: J. Alloy Compd., *315*, 2001, p. 211. doi:10.1016/S0925-8388(00)01267-6
[6] Suganuma, K., Niihara, K. J.: Mater Res., *13*, 1998, p. 2859. doi:10.1557/JMR.1998.0391
[7] Ohtani, H., Miyashita, M., Ishida, K.: J. Jpn Inst Met., *63*, 1999, p. 685.

[8] Suganuma, K., Murata, T., Noguchi, H., Toyoda, Y.: J. Mater Res., *15*, 2000, p. 884. doi:10.1557/JMR.2000.0126
[9] Vassilev, G. P., Tedenac, J. C., Dobrev, E. S., Evtimova, S. K.: Arch Metal., *46*, 2001, p. 249.
[10] Vassilev, G. P., Evtimova, S. K., Tedenac, J. C., Dobrev, E. S.: J. Alloy Compd., *334*, 2002, p. 182. doi:10.1016/S0925-8388(01)01778-9
[11] Date, M., Shoji, T., Fujiyoshi, M., Sato, K., Tu, K. N.: Scripta Mater., *51*, 2004, p. 641. doi:10.1016/j.scriptamat.2004.06.027
[12] Kim, K. S., Yang, J. M., Yu, C. H., Jung, I. O., Kim, H. H.: J. Alloy Compd., *379,* 2004, p. 314. doi:10.1016/j.jallcom.2004.03.138
[13] Song, J. M., Liu, P. C., Shih, C. L., Lin, K. L.: J. Electron Mater., *34*, 2005, p. 1249. doi:10.1007/s11664-005-0270-7
[14] Yu, D. Q., Xie, H. P., Wang, L.: J. Alloy Compd., *385*, 2004, p. 119. doi:10.1016/j.jallcom.2004.04.129
[15] Chonan, Y., Komiyama, T., Onuki, J., Urao, R., Kimura, T., Nagano, T.: Mater. Trans., *43*, 2002, p. 1887. doi:10.2320/matertrans.43.1887
[16] Chuang, C. M., Shih, P. C., Lin, K. L.: J. Electron. Mater., *33*, 2004, p. 1. doi:10.1007/s11664-004-0286-4
[17] Allen, S. L., Notis, M. R., Chromik, R. R., Vinci, R. P.: J. Mater. Res., *19*, 2004, p. 1425. doi:10.1557/JMR.2004.0191
[18] Tsai, J. Y., Hu, Y. C., Tsai, C. M., Kao, C. R.: J. Electron. Mater., *32*, 2003, p. 1203. doi:10.1007/s11664-003-0012-7
[19] Wang, J., Zhang, L. G., Liu, H. S., Liu, L. B., Jin, Z. P.: J. Alloy Compd., *455*, 2008, p. 159. doi:10.1016/j.jallcom.2007.01.024
[20] Liang, J., Gollhardt, N., Lee, P. S., Schroeder, S. A., Morris, W. L.: Fatigue Fract. Eng. M., *19*, 1996, p. 1401. doi:10.1111/j.1460-2695.1996.tb00175.x
[21] Vianco, P. T., Rejent, J. A., Kilgo, A. C.: J. Electron. Mater., *33*, 2004, p. 1373. doi:10.1007/s11664-004-0167-x
[22] Liang, J., Downes, S., Dariavach, N., Shangguan, D., Heinrich, S. M.: J. Electron. Mater., *33*, 2004, p. 1507. doi:10.1007/s11664-004-0092-z
[23] Liang, J., Dariavach, N., Barr, G., Fang, Z.: J. Electron. Mater., *35*, 2006, p. 372. doi:10.1007/BF02692459
[24] Seo, S.-K., Kang, S. K., Shih, D.-Y., Lee, H. M.: Microelectron. Reliab., *49*, 2009, p. 288. doi:10.1016/j.microrel.2008.11.014
[25] Hansen, M., Anderko, K.: Constitutions of Binary Alloys. 2nd edn. New York, McGraw-Hill 1985.
[26] Gunduz, M., Hunt, J. D.: Acta Metall., *33*, 1985, p. 1651. doi:10.1016/0001-6160(85)90161-0
[27] Gunduz, M., Hunt, J. D.: Acta Metall., *37*, 1989, p. 1839. doi:10.1016/0001-6160(89)90068-0
[28] Maraşli, N., Hunt, J. D.: Acta Mater., *44*, 1996, p. 1085. doi:10.1016/1359-6454(95)00227-8
[29] Touloukian, Y. S., Powell, R. W., Ho, C. Y., Klemens, P. G.: Thermal Conductivity Metallic Elements and Alloys. Vol. 1. Washington, New York 1970, p. 404.
[30] Touloukian, Y. S., Powell, R. W., Ho, C. Y., Klemens, P. G.: Thermal Conductivity Metallic Elements and Alloys. Vol. 1. Washington, New York 1970, p. 346.
[31] Terada, Y., Ohkubo, K., Mohri, T., Suzuki, T.: J. Alloy Compd., *285*, 1999, p. 233. doi:10.1016/S0925-8388(98)01042-1
[32] http://www.rrcap.unep.org
[33] Sergent, E. J., Krum, A.: Thermal Management Handbook: for Electronic Assemblies. Columbus, OH, McGraw Hill, Chapter 7, 1998.
[34] http://www.ndt-ed.org
[35] Frear, D., Morgan, H., Burchett, S., Lau, J.: The Mechanics of Solder Alloy Interconnects. New York, Van Nostrand Reinhold 1994.
[36] Mhiaoui, S., Sar, F., Gasser, J. G.: J. Non-Cryst Solids, *353*, 2007, p. 3628. doi:10.1016/j.jnoncrysol.2007.05.163
[37] Çadirli, E., Şahin, M., Kayali, R., Ari, M., Durmuş, S.: J Mater Sci: Mater Electron, *22*, 2011, p. 1709. doi:10.1007/s10854-011-0350-9
[38] http://environmentalchemistry.com
[39] Hultgren, R., Orr, R. L., Anderson, P. D., Kelley, K. K.: Selected Values of Thermodynamic Properties of Metals and Alloys. Berkeley, University of California, Johnson Wiley & Sons, Inc. 1963, p. 260.
[40] http://www.tf.uni-kiel.de
[41] Kaban, I., Khalouk, K., Köhler, M., Hoyer, W., Gasser, J. G.: J. Electron. Mater., *39*, 2010, p. 70. doi:10.1007/s11664-009-0952-7
[42] Kang, S. K., Horkans, J., Andricacos, P. C., Carruthers, R. A.: In: Proc. 49th Electronic Compounds Technology Conf. (Piscataway, NJ: IEEE), 1999, p. 283.
[43] Boyer, H. E., Gall, T. L.: Metals Handbook. Metals Park, OH, ASM International 1985, p. 44.
[44] Cook, B. A., Anderson, I. E., Harringa, J. L., Terpstra, R. L.: J. Electron. Mater., *31*, 2002, p. 1190. doi:10.1007/s11664-002-0009-7
[45] Babaghorbani, P., Nai, S. M. L., Gupta, M.: J. Alloy Compd., *478*, 2009, p. 458. doi:10.1016/j.jallcom.2008.11.074
[46] Kamal, M., Gouda, E. S.: J. Mat. Sci: Mater. Electron., *19*, 2008, p. 81. doi:10.1007/s10854-007-9289-2
[47] Wu, Y. K., Lin, K. L., Salam, B.: J. Electron. Mater., *38*, 2009, p. 227. doi:10.1007/s11664-008-0589-y
[48] Šebo, P., Štefánik, P.: Kovove Mater., *43*, 2005, p. 202.